 doi:10.20944/preprints201608.0206.v1

Article

Short-Range Vital Signs Sensing Based on EEMD and CWT Using IR-UWB Radar

Xikun Hu and Tian Jin *

College of Electronic Science and Engineering, National University of Defense Technology, Changsha 410073, China; xikung_hu@126.com

* Correspondence: tianjin@nudt.edu.cn

Abstract: The designed radar sensor realizes the healthcare monitoring capable of short-range to detect the chest-wall movement of the subject caused by cardiopulmonary activities, and wirelessly estimating the distance from the sensor to the subject without any devices being attached to the body. Ensemble empirical mode decomposition (EEMD) based denoise method and 1-D continuous-wavelet transform (CWT) are applied for improving on the detection SNR so that accurate respiration rate and heartbeat rate can be acquired in time domain or frequency domain with further distance. No choosing the conventional Doppler radar only able to capture the Doppler signatures due to the lack of bandwidth information as noncontact sensor, we take full advantages of ultra-wideband (UWB) impulse radar to make it low power consumed and portable conveniently, with flexible detection range and preferable accuracy. This noncontact healthcare sensor system addressed proves the commercial feasibility and vast availability of using compact impulse radar for emerging biomedical applications. Compared with traditional contact measurement devices, experimental results utilizing the 2.3 GHz bandwidth transceiver, demonstrate 100% similar results.

Keywords: impulse radar; ultra-wideband (UWB); noncontact; short-range; healthcare; respiration; heartbeat; SNR; ensemble empirical mode decomposition (EEMD); continuous-wavelet transform (CWT)

1. Introduction

Radar sensor has been widely used in a number of applications since 1930s [1], from primary vehicle speed measurement to the advanced air-defense and marine radars, all of which are usually developed for detecting, targeting, and even tracking moving subjects at large distances. Due to the noninvasive and noncontact specialties, short-range radar has been appealing in healthcare applications since 1970s, when the first short-range non-invasive microwave sensor for respiration measurement was introduced [2]. Because of the radar operation based on the principle of electromagnetic backscattering [3], radar is capable of both wirelessly detecting the chest-wall movements caused by respiration and extremely small heart beating, on the other hand, conventional medical devices like electrocardiograph (ECG) and respiration belt can only rely on electrodes and an inductive plethysmograph, which make the subjects uncomfortable, even worsen the physiological measure. For instance, in the long time monitoring (obstructive sleep / coma subject), an alarm connected with radar processor would be triggered to either awake the subject or message the subject's nursing assistants so they can take measures immediately to avoid possible danger or accident [4]. In contrast, the wearable devices demand the subject attaching to electric poles twisted with several wires for heartbeat monitoring or vacuum belt for respiratory monitoring during sleep, which may have a negative impact on sleeping quality [5]. Despite the benefits it brings, the wide implementation of non-contact physiological detectors in practical clinical applications was limited and even stopped in the past years due to the concern for human safety under the high power radiation, as well as bulkiness of the apparatus and high cost [6].

Ultra-wideband (UWB) radar is a technology for transmitting electromagnetic wave spread over a large bandwidth (normally larger than 500MHz). Usually, most of UWB radars transmit via large bandwidth over short pulse periods, typically on the order of a nanosecond, or even picosecond, for which we generally refer to this type of UWB signaling as impulse radio UWB (IR-UWB) radar [7,8]. The nature of IR-UWB radar makes it more power-efficient, higher range resolution and higher detection accuracy than other traditional radar systems like continuous-wave (CW) radar and frequency-modulated continuous-wave (FMCW) radar [9,10]. Because of these superior specificities, it has gained popularity in social and military applications such as searching for earthquake or fire victims, detecting the presence of a human in border patrol, assisting the entrance security, even hunting indoor terrorists using through-the-wall radar [11,12]. With growing interest of employing radar sensors for practical clinical applications, many researches have been pushing the UWB technology boundaries in every aspect to try to make its applications ubiquitous in our daily lives, owing to the advantages like high range resolution, high data rate, low transmit power and low interference [11]. These characteristics make IR-UWB radar more attractive for noncontact vital sign detection, because it is capable of measuring absolute distance with high resolution and better materials-penetrating performance [13], while CW radar can only rely on Doppler information to track relative movements due to lack of modulated spectral information [3]. Together given that FMCW dramatically increases the complexity of the radar hardware system and signal processing approaches, even though it can detect both absolute distance and relative displacement movements [14], IR-UWB radar is a better option. In addition, as the advancement of system integration chip technologies, the nano-scale UWB impulse radar transceiver chip has been developed recent years, realizing the superfast sampling rate around 39 GS/s with low-power consumption [15], which makes them more attractive for mobile, portable, and even handheld applications in future trends.

McEwan made a first try of applying IR-UWB radar in medical applications for human body monitoring and imaging in 1993. Next, the relevant first US Patent application was filed for medical UWB radar in 1994, and then rewarded in 1996 [16]. At the same year, “Radar Stethoscope”, an educational project was put through by MIT [17]. Since then, UWB is often considering as a possible alternative to medical remote sensing and medical imaging. U.S. patents emphasize that, for the continuous human exposure to microwave, the average emission level used (1μW) is about 3rd orders of magnitude lower than most international standards making devices medically harmless, which accelerates the development of UWB radar in the field of biomedicine [18].

Since 21st century, several radar prototypes based on IR-UWB radar for noncontact vital signs detection have been fundamentally realized [19-26]. In 2010, Lazaro et al. realized non-invasive monitoring of breathing and heartbeat rates using the independently complex generator and sampler, which inevitably made it heavy [23]. To decrease the weight of Radar system, , Khan et al., in 2014, made it feasible to monitor the vital sign of a non-stationary human using IR-UWB transceiver chip NVA6201, which also provide an novel way for us to further study, but it did not optimize the complete implementation procedures from signal modeling to experimental results under different measurement setups and scenarios [24]. Besides, in 2015, Huang et al. utilized other kind of UWB radar chip, the Time Domain's PulsON400, to monitor the infant respiration, but no referring to heartbeat detection [25]. Typically, in relaxed human beings the heart can cause chest displacements of 0.08 mm, and respiration displacements of between 0.1 mm and several millimeters, depending on the person [26], and the spectrum of the detected signal contains several harmonics of the breathing signal that can be much stronger than the frequency component of the heartbeat [23]. Therefore, it will be more difficult to extract heartbeat signals from complicated radar echo signals. In this paper, using an IR-UWB Radar, the breathing rate and heartbeat frequency are separated and detected remotely and estimated based on EEMD-CWT algorithm.

This paper focuses on the theoretical and experimental vital sign detection based on a new method of EEMD-CWT. The key idea on the EEMD relies on averaging the modes obtained by EMD applied to several realizations of Gaussian white noise added to the original signal [28-29]. But in [30], a particular noise is added at each stage of the decomposition and a unique residue is

 doi:10.20944/preprints201608.0206.v1

computed to obtain each mode. The resulting decomposition is complete, with a numerically negligible error, which can be utilized to denoise the signal after clutter suppression. And then a Morlet wavelet transform is used to reconstruct the respiratory signal and heartbeat signal.

The remainder of this paper is organized as follows. Section 2 presents mathematical model of vital sign. The signal processing techniques used to detect the respiration and heart rates are presented in Section 3. We describe the IR-UWB sensor system and experimental setup in Section 0. In Section 5, Experiments results and comparisons are presented. Section 6 concludes this paper.

2. Mathematical Model of Vital Sign

Before designing a sensor system, it is necessary to make them clear about what the signal model is, how the signal propagates and how to receive and detect the echo signal effectively. The section below demonstrates that it is of vital importance to make this complete analysis, for the large amplitude of breath harmonics makes heart rate measurement a challenge [21], especially when they are close to the heart frequency, which may be the first challenge that hinders the ubiquitous use of radar technology.

By observing the changes of propagating time delay of echo signal from the subject, we can detect the vital sign remotely. When the transmitted pulse illuminates the human subject, part of it is reflected back to the radar because of the high reflectivity of the body [19]. And the time-of-flight of this pulse is denoted by τ_0, depending on the antenna distance d_0. The subject's chest wall movement induced by the respiration and heartbeat modulates the reflected signal. Because of respiration and heart motion, the chest cavity expands and contracts periodically, so the distance travelled, $d(t)$, varies periodically around the nominal distance d_0. In other words, the distance between the antenna and the human chest varies approximately as harmonic vibration, which is expressed as:

$$d(t) = d_0 + m(t) = d_0 + m_r \sin(2\pi f_r t) + m_h \sin(2\pi f_h t) \tag{1}$$

where t is slow-time, m_r and m_h are the displacement amplitudes of the respiration and heartbeat, respectively, f_r and f_h are the frequencies of the respiration and heartbeat, respectively.

First, we assume that all targets illuminated by the antennas radiation pattern are stationary excluding the light cardiopulmonary motion of the subjects, and the impulse response of the radar is:

$$r(t,\tau) = \sum_i a_i \delta(\tau - \tau_i) + a_v \delta(\tau - \tau_v(t)) \tag{2}$$

where $\delta(t)$ is the normalized received pulse, and $\sum_i a_i \delta(\tau - \tau_i)$ corresponds to the reflections of the static background targets, a_i is the amplitude of each multipath component, t_i its propagation time delay of i-th static target reflection in fast-time. a_v is the amplitude of the pulse on the body. The time delay $\tau_v(t)$ associated with the vital sign is the propagation time delay of subject reflection in fast-time, and t presents the slow-time on which the echo signal is obtained. $\tau_v(t)$ can be calculated as below:

$$\tau_v(t) = \frac{2d(t)}{c} = \tau_0 + \tau_r \sin(2\pi f_r t) + \tau_h \sin(2\pi f_h t) \tag{3}$$

where c is the light velocity, and τ_r and τ_h are the respiration displacements and heartbeat displacements, respectively, $\tau_0 = 2\,d_0/c$, $\tau_r = 2\,m_r/c$ and $\tau_h = 2\,m_h/c$. Let $s(t)$ represent the transmitted signal, and then the received signal is:

$$R(\tau,t) = s(\tau) * r(t,\tau) = \sum_i a_i s(\tau - \tau_i) + a_v s(\tau - \tau_v(t)). \tag{4}$$

For digital signal processing, the received waveforms are measured at discrete instants in slow-time $t = nT_s$ ($n = 0,1,\ldots N-1$), where T_s is the pulse repetition time. N discrete-time sequences are stared after the received signal is sampled. The discrete signal can be expressed as an $M \times N$ matric $\boldsymbol{R}$ the element of which are:

$$R[n,m] = r\left(\tau = mT_f,\, t = nT_s\right) = \sum_i a_i s\left(mT_f - \tau_i\right) + a_v s\left(\tau - \tau_v\left(nT_s\right)\right) \tag{5}$$

Preprints (www.preprints.org) | NOT PEER-REVIEWED | Posted: 25 August 2016 doi:10.20944/preprints201608.0206.v1

where T_f is the sampling period in fast-time, and $m = 0,1,\ldots,M-1$ is the fast-time sampling points.

In a static environment, the clutter can be considered as a DC-component in the slow-time direction. As a result, the only movement is caused by the cardiopulmonary respiration and heart activity, from (2) it is clear that background clutter does not depend on slow-time t. Thus, we can use basic filter to remove the background clutter, which can be easily done by subtracting the mean from the matric $\boldsymbol{R}$. After subtraction, there will be only one received signal remained [23], which can be expressed as:

$$x(t,\tau) = r(t,\tau) - \lim_{T\to\infty}\frac{1}{T}\int_0^T r(t,\tau)dt = a_v s(\tau - \tau_v(t)) - r_0(\tau). \tag{6}$$

The DC component $r_0(\tau)$ is blocked by subtracting the average of all samples in fast-time.

According to (6) we can get the signal if interest without any stationary background as below:

$$y(t,\tau) = a_v s(\tau - \tau_v(t)). \tag{7}$$

From (3) and (4), we can update (7) as below:

$$y(t,\tau) = a_v s(\tau - \tau_v(t)) = a_v s(\tau - \tau_0 - \tau_r \sin(2\pi f_r t) + \tau_h \sin(2\pi f_h t)). \tag{8}$$

In order to estimate the respiratory frequency f_r and heartbeat f_h, the Fourier transform of (8) is performed in slow-time $Y(f,\tau)$.

$$\begin{aligned} Y(f,\tau) &= \int_{-\infty}^{+\infty} y(t,\tau)e^{-j2\pi ft}dt \\ &= \int_{-\infty}^{+\infty} Y(f,v)e^{j2\pi ft}dv \end{aligned}. \tag{9}$$

where $Y(f,v)$ is the 2-D Fourier transform of (8), which is given by:

$$\begin{aligned} Y(f,v) &= \int_{-\infty}^{+\infty}\int_{-\infty}^{+\infty} y(t,\tau)e^{-j2\pi ft}e^{-j2\pi v\tau}dtd\tau \\ &= \int_{-\infty}^{+\infty} a_v P(v)e^{-j2\pi v\tau_d(t)}e^{-j2\pi ft}dt \\ &= a_v P(v)e^{-j2\pi v\tau_0}\int_{-\infty}^{+\infty} e^{-j2\pi v m_r \sin(2\pi f_r t)}e^{-j2\pi v m_h \sin(2\pi f_h t)}e^{-j2\pi ft}dt \end{aligned} \tag{10}$$

where $P(v)$ is the Fourier transform of (8) in fast-time index. Refer to [21] and use the following expansion of Bessel series:

$$e^{-jz\sin(2\pi f_0 t)} = \sum_{k=-\infty}^{+\infty} J_k(z)e^{-j2\pi kf_0 t}. \tag{11}$$

Then the (10) can be expressed as:

$$\begin{aligned} Y(f,v) = a_v P(v)e^{-j2\pi v\tau_0}\int_{-\infty}^{+\infty}\Big(\sum_{k=-\infty}^{+\infty} J_k(\beta_r \mathrm{v})e^{-j2\pi kf_r t}\Big) \\ \cdot\Big(\sum_{l=-\infty}^{+\infty} J_l(\beta_h \mathrm{v})e^{-j2\pi kf_h t}\Big)e^{-j2\pi ft}dt \end{aligned} \tag{12}$$

where $\beta_b = 2\pi m_r$ and $\beta_h = 2\pi m_h$. By replacing (12) in (9), the spectrum in slow-time is expressed as below:

$$Y(f,\tau) = a_v\sum_{k=-\infty}^{+\infty}\sum_{l=-\infty}^{+\infty} G_{kl}(\tau)\delta(f - kf_r - lf_h) \tag{13}$$

where $G_{kl}(l)$ can be represented by the intergrals:

$$G_{kl}(l) = \int_{-\infty}^{+\infty} P(v)J_k(\beta_r v)J_l(\beta_h v)e^{j2\pi v(\tau-\tau_0)}dv. \tag{14}$$

Preprints (www.preprints.org) | NOT PEER-REVIEWED | Posted: 25 August 2016 doi:10.20944/preprints201608.0206.v1

Apparently, $|G_{kl}(\tau)|$ is maximized at $\tau = \tau_0$:

$$G_{kl} \equiv G_{kl}(\tau_0) = \int_{-\infty}^{+\infty} P(v) J_k(\beta_r v) J_l(\beta_h v) dv \,. \tag{15}$$

So (13) can be rewritten as below:

$$Y(f,\tau) = a_v \sum_{k=-\infty}^{+\infty} \sum_{l=-\infty}^{+\infty} G_{kl} \delta(f - kf_r - lf_h) \,. \tag{16}$$

It is obvious to observe from (16) that the spectrum of signal in slow-time index is a discrete function, which consists of respiratory rate f_r, heartbeat rate f_h and a train of harmonics. The amplitude G_{kl} is related to the fast-time, and it controls the amplitude of each intermodulation product for a frequency of $f = kf_r + lf_h$.

The detection method will be introduced in the next section, which will be utilized in separating the vital signs.

3. Detection Algorithm

The slow-time signal is processed to obtain the breathing frequency f_h and heartbeat rate f_r. Considering spectrum of slow-time signal fully, in this section, we propose and elaborate the theory of a combined detection method based on a variation of EEMD algorithm and CWT analysis for impulse UWB signal module, after the clutter suppression using (6).

As the signal processing proposed in [31], facing the same problems of moving interference of the environment, the combined methods was proposed, which includes several ordinary methods of extracting periodic signal from noise, such as self-correlation, adaptive line enhancer (ALE), blind source separation (BBS), EMD, *etc.*, and concludes the effect is not obvious when only using one of the methods mentioned. For sensing the human subject outdoors in [31], it is necessary to remove interference continuously, so ALE is added to reduce the Gaussian noise signal of the detected respiration adaptively. But for the remotely sensing vital signs including not only the respiration but heartbeat, the higher SNR improvement is required. Therefore, the EEMD is introduced to improve the SNR of echo signal including respiration signal, heartbeat signal and noise. And then, after denoising, the separation algorithm CWT is used for extracting the weak heartbeat signal from echo signal. Figure 1 shows the block diagram of signal processing.

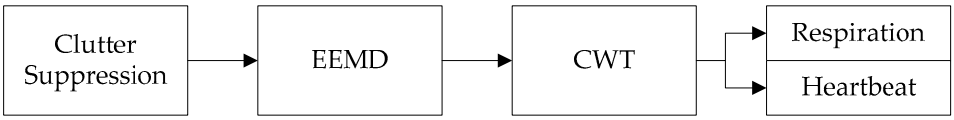

Figure 1. Proposed detection method.

Generally, finite impulse response (FIR) or infinite impulse response (IIR) filters can be used for cancelling noise and passing given frequency bandwidth to filter the ideal signals. Since the amplitude of respiration is much larger than that of the heartbeat, it is easy to observe periodic waves from the baseband output. But the pretty weak heartbeat would be overlapped by the noise within a passband. Therefore, this traditional method would fail in some degree. In order to check the improved performance by proposed method, a traditional processing method using a band-pass FIR filter to separate the vital signs is introduced in Figure 2. We made a comparative experimental presentation between the proposed method with the traditional FIR filtering method in terms of respiration and heartbeat, respectively. The filter passes signals below 0.5 Hz and blocks those beyond 0.65 Hz. According to the prior knowledge of the heartbeat frequency range that the normal heartbeat rate varies from 60 to 100 beats/min (about 1.0–1.6 Hz), to obtain the heartbeat signal, the frequency window is set to be 0.65–3.0 Hz with 656th order. To reject out-of-band noise and to obtain the respiration signal, a low-pass elliptic FIR filter is applied.

Preprints (www.preprints.org) | NOT PEER-REVIEWED | Posted: 25 August 2016 doi:10.20944/preprints201608.0206.v1

Figure 2. Traditional FIR filter method.

3.1. Clutter Suppression Algorithm

In a static environment, the clutter from the background can be considered as DC component and can be removed easily by subtracting the mean from the matrix $\boldsymbol{R}[\boldsymbol{n},\boldsymbol{m}]$ in (5), in both rows and columns. After subtraction, there will be only one received signal remained.

To suppress background stationary target, slow clutter and antenna crosstalk effect, summing and mean signal amplitudes along fast time range bin presents the strength of clutter as in (17) and due to the periodic amplitude cancellation, $x(t,\tau)$ contains little information of vital signs, which is simplified referring to as $x_{m,n}$ in time domain, presenting the n-th slow-time sample of the m-th range bins. In the fast-time domain, the detection range is divided into 256 bins. To obtain the position of target, maximum range bin is calculated to maintain the anticipate range gate, as described below:

$$v = \arg\max_{m}\left(\sum_{n=1}^{N}\left(x_{m,n} - \frac{1}{N}\sum_{n=1}^{N}x_{m,n}\right)^{2}\right) \tag{17}$$

where $n = 0,1,\ldots N-1$ represents the number of pulses, and $m = 0,1,\ldots,255$ is the number of range bins along the fast time. v represents the selected vital signs bin between 0-255, the slow-time signal $x_{v,n}$ is the vital signs signal along the slow-time. The flowchart of implementing measurement of respiration and heartbeat rate is shown in Figure 3.

Figure 3. Signal processing block diagram of clutter suppression.

3.2. Ensemble Empirical Mode Decomposition Denosing Algorithm

As definition in [28], EMD is an adaptive method used to analyze non-linear and non-stationary signals. In order to overcome some problems of EMD, such as oscillations of very disparate in a mode, or very similar oscillation in different modes, a new method was proposed: EEMD [29], which performs the EMD over an ensemble of the signal plus Gaussian white noise; however, it creates some new matters. The reconstructed signal including residual noise and different realizations of signal plus noise may produce different number of modes. Then, in 2011, a variation of the EEMD algorithm was proposed that provides an exact reconstruction of the original signal and a better spectral separation of the modes, with a lower computational cost [30].

EMD decomposes a signal $x(t)$ into a (usually) small number of Intrinsic Mode Functions (IMFs) or modes. To be considered as an IMF, a signal must satisfy two conditions: (i) the number of extrema and the number of zero crossing must be equal or differ at most by one; and (ii) the mean value of the upper and lower envelope is zero everywhere. EEMD defines the "true" IMF components (here notated as $\overline{IMF}$ in what follows) as the mean of the corresponding IMFs obtained via EMD over an ensemble of trials, generated by adding different realizations of white noise of finite variance to the vital signs signal.

To achieve good contrast, we describe the EEMD proposed by Huang et al. as Figure 4 showed, and the improved EEMD algorithm used to denoise processing by Flandrin et al. in Figure 5, which has a better spectral separation of the modes, with a lower computational cost. Although EEMD alleviates the mode mixing, it is still too much time consuming because of the large number of sifting iterations required to achieve the decomposition. In addition, a fundamental frequency extraction algorithm could fail to identify the mode that contains it when applied to EEMD

Preprints (www.preprints.org) | NOT PEER-REVIEWED | Posted: 25 August 2016 doi:10.20944/preprints201608.0206.v1

decomposition. The method here used has the advantages of requiring less than half the sifting iterations that EEMD does, and that the original signal can be exactly reconstructed by summing the modes.

After denoising, the echo signal $x[n] = x_{v,n}$ obtained by (17) can be rewritten in the n-th slow-time:

$$x[n] = \sum_{k=1}^{K} IMF_k \tag{18}$$

without the residue, and on the other hand, we can choose several not all of IMFs from $k = 1, \dots, K$ to reconstruct out ideal echo signal.

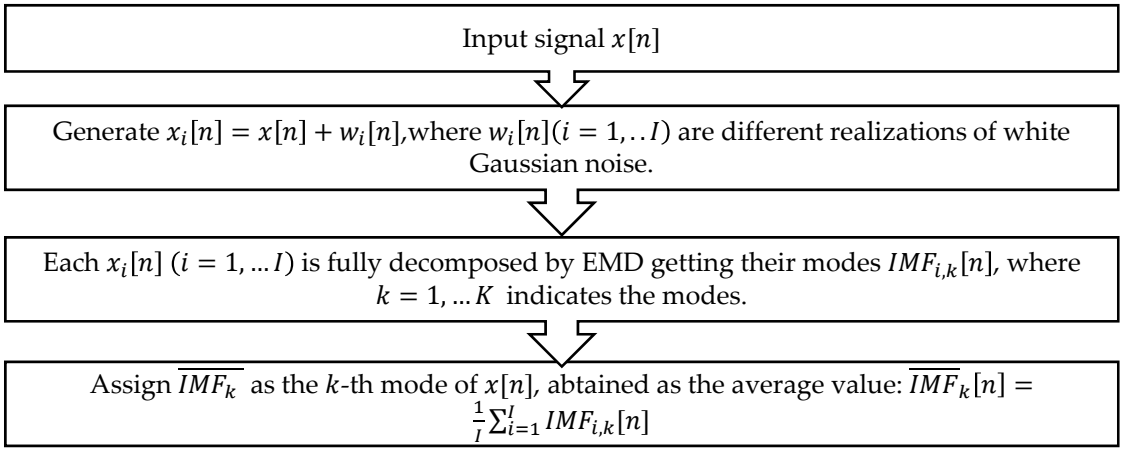

Figure 4. Flowchart of EEMD.

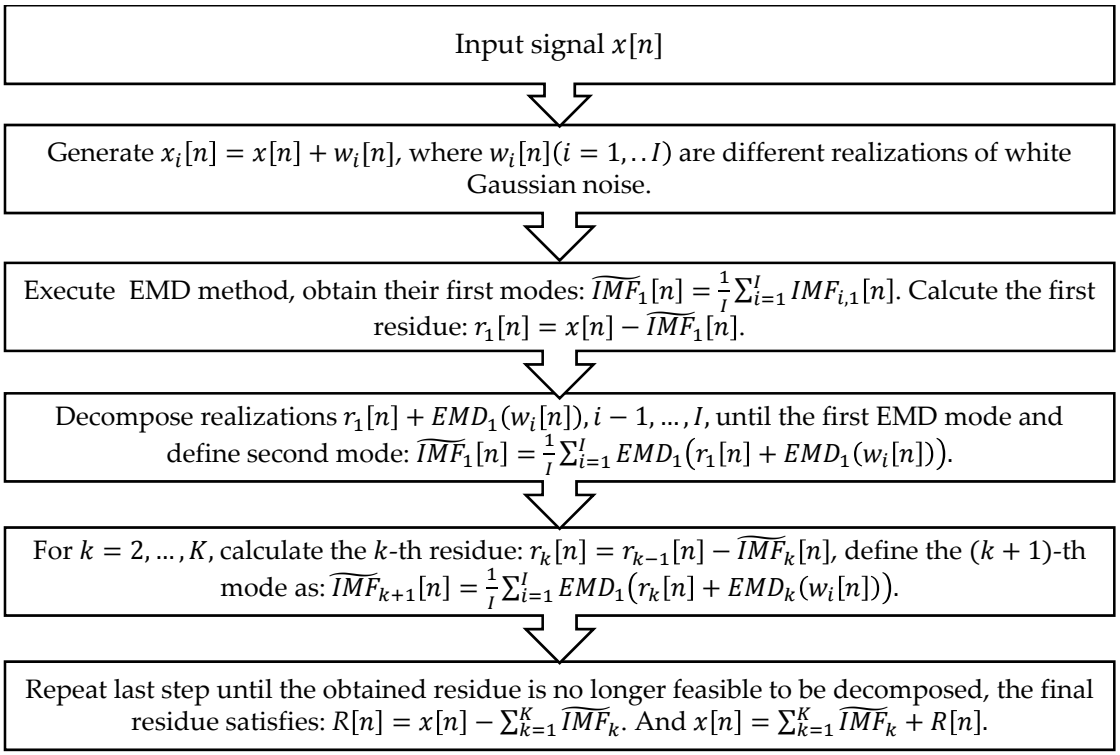

Figure 5. Flowchart of a variance of EEMD.

3.3. Continuous Wavelet Transform Algorithm for Separating Vital Signs

After denosing, the SNR of signal is enhanced. However, for a signal with low SNR, especially for heartbeat signal, it is still difficult to separate the respiration and heartbeat. The proposed

Preprints (www.preprints.org) | NOT PEER-REVIEWED | Posted: 25 August 2016 doi:10.20944/preprints201608.0206.v1

algorithm in this paper to find the respiration rate and heartbeat rate, is based on the computation and then comparison of the filter bank sub-bands' energy. Particularly, wavelet filter banks are used because of their capability to find the energy in the desired frequency interval. Wavelets provide excellent time resolution for rapid events such as heartbeats and good frequency resolution for slower events such as respiration.

First, we introduce the signal analysis methods, from the frequency analysis method of Fourier transform (FT) to time-frequency ones like short time Fourier transform (STFT) and CWT, which are variances from FT. Like the FT, the CWT uses inner products to measure the similarity between a signal and an analyzing function. In the FT, the analyzing functions are complex exponentials $e^{-j\omega t}$. The resulting transform is a function of a single variable, ω. In the STFT, the analyzing functions are windowed complex exponentials, $w(t)e^{j\omega t}$, and the result in a function of two variables. The STFT coefficients, $F(\omega,\tau)$, represent the match between the signal and a sinusoid with angular frequency ω in an interval of a specified length centered at τ. In the CWT, the analyzing function is a wavelet, ψ. The CWT compares the signal to shifted and compressed or stretched versions of a wavelet. Stretching or compressing a function is collectively referred to as dilation or scaling and corresponds to the physical notion of scale. By comparing the signal to the wavelet at various scales and positions, you obtain a function of two variables. If the wavelet is complex-valued, the CWT is a complex-valued function of scale and position. If the signal is real-valued, the CWT is a real-valued function of scale and position. For a scale parameter, $a > 0$, and position, b, the CWT is:

$$C(a,b;f(t),\psi(t)) = \int_{-\infty}^{\infty} f(t)\frac{1}{\sqrt{a}}\psi^{*}(\frac{t-b}{a})dt \tag{19}$$

where $*$ denotes the complex conjugate. Not only do the values of scale and position affect the CWT coefficients, the choice of wavelet also affects the values of the coefficients.

The CWT employed in this paper can be regarded as processing denoised signal using a bank of filters successively. Morlet wavelet was chosen as the mother wavelet because of its wide applications in the ECG to discriminate the abnormal heartbeat behavior [35]. And thorough experimental results, the Morlet wavelet works better than other wavelets. The application of the wavelet filter decomposes the signal into a series of components, and for each decomposition levels, the coefficients can be either set to zero or reduced in magnitude, so that a particular feature of the signal is affected on reconstruction. The high-frequency (HF) components are used for heartbeat signal recovery and the low-frequency (LF) ones for respiration recovery. Finally, a moving average filter is applied to each signal, thus the heartbeat and respiration signal are reconstructed. The signal processing proposed for recovering ideal signals can be summarized as Figure 6.

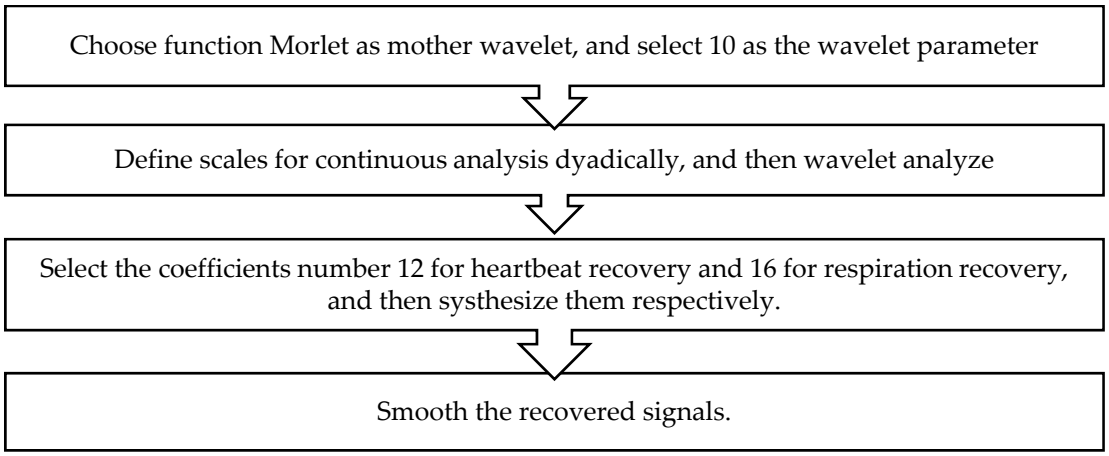

Figure 6. Flowchart of Morlet CWT.

Preprints (www.preprints.org) | NOT PEER-REVIEWED | Posted: 25 August 2016 doi:10.20944/preprints201608.0206.v1

4. Radar System and Experimental Setup

4.1. Radar System

The design of sensors is based on impulse radar NVA series 661 (Novelda, Norway) being fully integrated nano-scale radar transceivers, with the low-power energy consumption. It also provides flexible control of the key parameters, such as pulse repetition frequency (PRF), sampling rate, and the samplers per frame.

The chip (NVA6201) employs a novel technology called "Continuous Time Binary Value" (CTBV), which can solve part of main problems of traditional sampling methods by excluding the demand for a high-resolution ADC while realizing an impressive time resolution of modern digital circuits. The sampling chain is realized using inherent gate-delays resulting in a rate of about 39 GS/s for a single frame, which consists of maximum 512 samples. See for example [33] for an introduction to the implemented sampling technology.

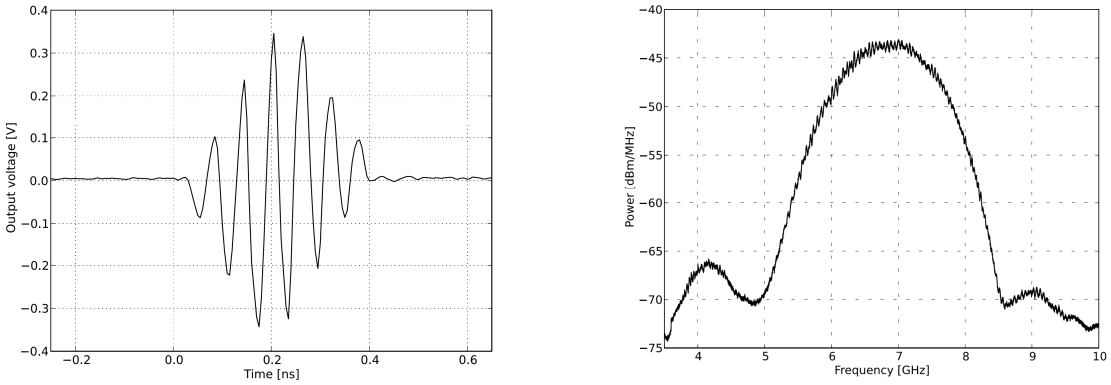

Figure 7. Transmitted Signal in time domain and frequency domain. (**a**) Pulse generator time domain output; (**b**) Pulse generator output spectra.

It is the pulse generator to transmit the narrow Gaussian pulse signal whose derivative of approximation is 11 as Figure 7 (a) displayed, with PRF 100 MHz and with highly configurable output frequency band, as Figure 7 (b) showed. After enhancing by the power amplifier, the signal is emitted by transmitting Vivaldi antennas, which can be easily observed in Figure 8. In the receiver, the reflected echo is firstly received by the receiving antennas and then magnified by a low-noise amplifier (LNA). After that, the signal containing the information of vital signs is sampled by the high speed sampler after a fixed offset in sequence with the fast-time sampling frequency about 39 GHz. Finally, the digital signal is transferred to the MATLAB processor on a computer with the slow-time frequency about 200 Hz. The whole energy consumed for one measurement is less than 120 mW [34].

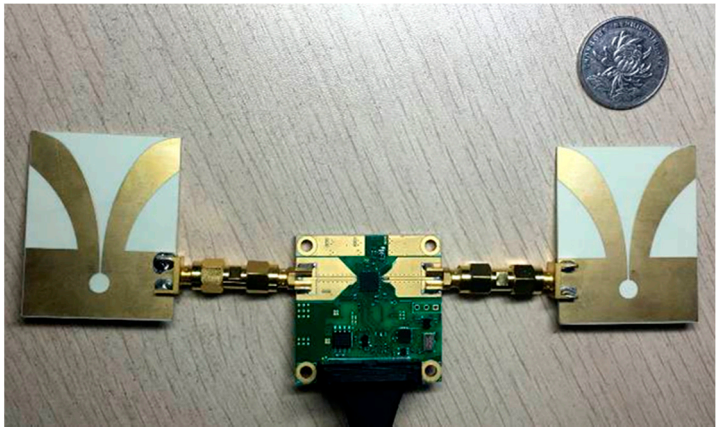

Figure 8. NVA661 nano-scale IR-UWB Radar.

Preprints (www.preprints.org) | NOT PEER-REVIEWED | Posted: 25 August 2016 doi:10.20944/preprints201608.0206.v1

4.2. Experimental Setup

Figure 9 shows the experimental setup of the radar for measurement. The volunteer is a 22-year-old healthy male, sitting in a chair and breathing regularly with the medical devices monitoring simultaneously, with around 0.3 m from antennas to the volunteer as Figure 9(a) showed.

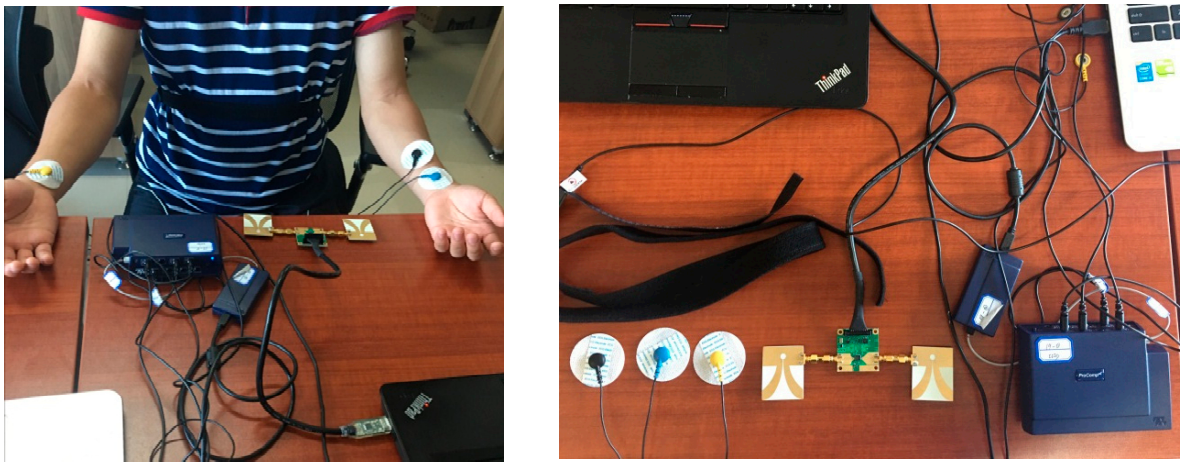

(**a**) (**b**)

Figure 9. Experimental setup. (**a**) Experimental scenario. (**b**) The radar sensor and DynaMap Suite.

The specification for the measurement is represented in Table 1. In order to evaluate the performance of the radar system, we apply a comprehensive sports medicine tool (DynaMap Suite – SA7925, Thought Technology Ltd., Montreal West, Canada) as Figure 9(b) showed, which can monitor several medical indexes consisting of ECG, HR, IBI, and respiration, *etc*., using the BioGraph Infiniti Software to capture and export the respiratory data and ECG data, as the measurement references.

Table 1. Specifications for the measurement.

Parameters	Speecifications
Antennas	Vivaldi
Center Frequency	6.8 GHz
Bandwidth	2.3 GHz
Number of points	256 points
Distance between antennas and the target	0.3 m
Height of antennas	0.8 m
Distance between antennas	0.1 m
The target's stance	Sitting on a chair
Average measuring time	0.55 s
Power consumption	120 mW

5. Results

5.1. SNR Comparison of FIR Filter and Proposed Method

Figure 10(a) refers to the original vital signs obtained after clutter suppression. From the respiration waveforms in Figure 10(b) and Figure 10(c), it is easy to read the respiration rates, since its peak and valleys are quite obvious, but the respiration signal obtained using proposed method has a more legible tendency and more defined signatures than the one using FIR filter from their respective waveforms in time domain. On the other hand, due to lower reflected energy heartbeat

Preprints (www.preprints.org) | NOT PEER-REVIEWED | Posted: 25 August 2016 doi:10.20944/preprints201608.0206.v1

waveforms in Figure 10(d) have just about 0.2 mV peak-peak values, and the waveform obtained using FIR filter displays an irregular sign, without any unambiguous heartbeat tendency, whereas the waveforms decomposed results using proposed method have a stable and regular heartbeat waveform shown in Figure 10(e). Above all, the proposed method works better than traditional FIR method in sensing vital signs.

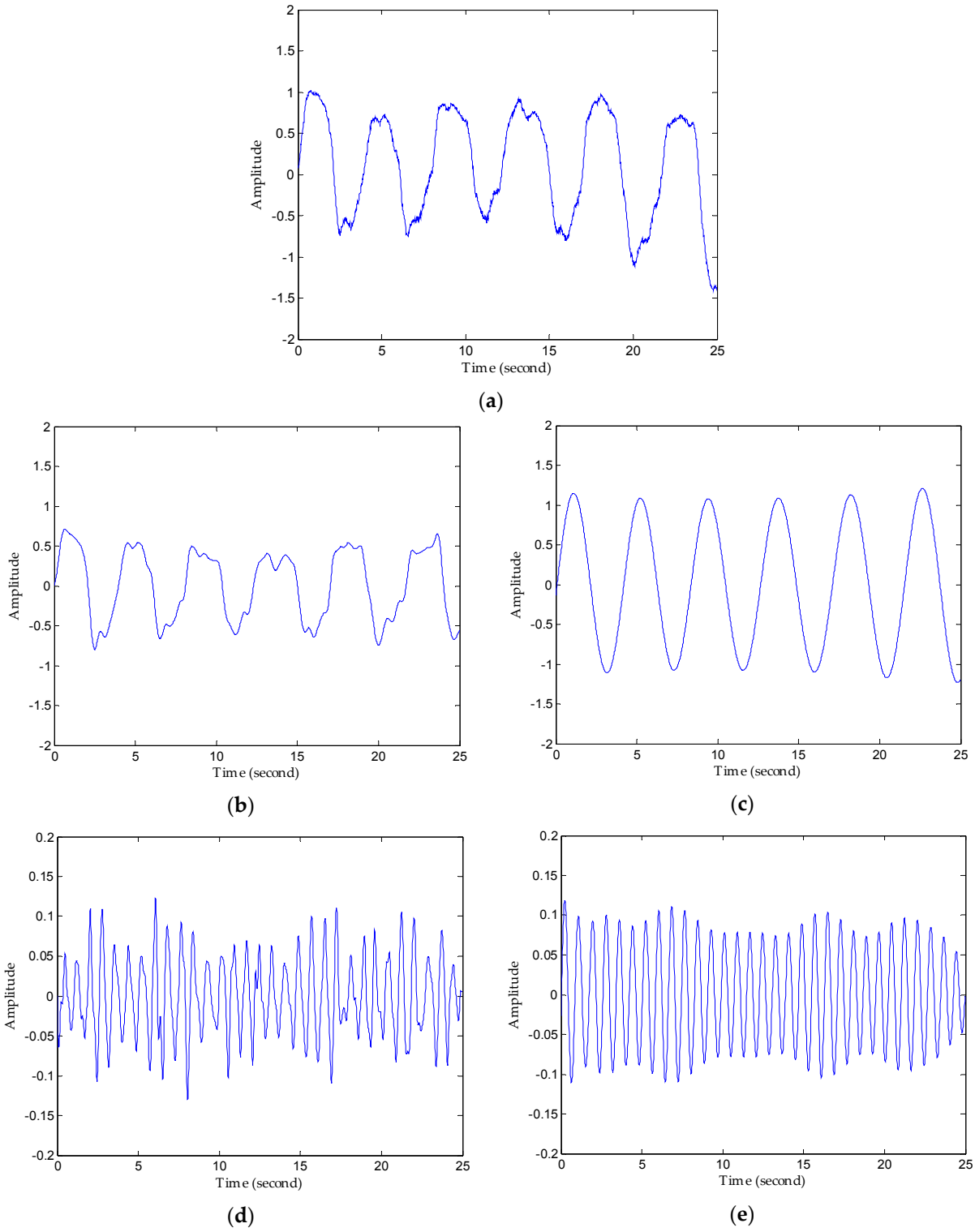

Figure 10. Comparison of results using FIR filter and proposed method. (**a**) The original waveforms obtained after clutter suppression. (**b**) Respiration waveforms obtained via FIR band-pass filter. (**c**) Respiration waveforms obtained via the proposed method. (**d**) Heartbeat waveforms obtained via FIR band-pass filter. (**e**) Heartbeat waveforms obtained the proposed method.

Preprints (www.preprints.org) | NOT PEER-REVIEWED | Posted: 25 August 2016 doi:10.20944/preprints201608.0206.v1

For the quantitative analysis, SNR calculations and detection results of respiration and heartbeat are shown in Table 2. The average SNR improvement of respiration detection by the method described in this paper is 7.59 dB, besides that, the average SNR improvement of heartbeat signals is 4.82 dB. Using the proposed method, the higher SNR can contribute to improving detection accuracy at more complex environments, and increasing the detection range in some degree, which can help IR-UWB radar adapt in many different environments and even with different human postures. And it is well-known that higher SNR is of vital importance for radar system, which helps decrease the false alarm probability, especially significantly for the medical monitoring applications in the future trends.

Table 2. SNR of respiration rate and heartbeat rate using FIR filter and proposed method.

Parameters	Radar	
	FIR	Proposed Method
SNR of Respiration	4.44 dB	12.03 dB
SNR of Heartbeat	-53.52 dB	-48.70 dB

5.2. Detection Performance of Proposed Method

Using the proposed method, first of all, we managed to denoise the signal, and then make it easy to analyze using CWT method. As Figure 11(a) presented, it can be seen obviously that the noise attached to the signal has been removed after the denosing processing using an algorithm based EEMD from the enlarged view. The noise IMFs contains the ahead 4 IMFs, as Figure 11(b) showed, which means the reconstructed signal we obtain is coming from last 8 IMFs. Then, we used the wavelet toolbox to analyze the denoised signal and choose the 12nd scales to synthesize the respiration signal and 16th for heartbeat signal effectively. The results of signal separation can be found in Figure 12, from which we can observe that accurate respiration signal waveform and exact heartbeat signal waveform can be obtained using proposed method. Finally, after that we extracted the heartbeat and respiration waveform. The examples of 20 s extracted heartbeat signal and ECG reference signal are compared in Figure 13(a), and 120 s extracted respiration signal and respiration reference signal are compared in Figure 13(b). The results show that the heartbeats superimposed on the respiration can be decomposed with clearly seen peaks and corresponds with the ECG, and the respiration decomposed results also show a high consistency with the reference signal. The proposed method realized a comparable detection performance with professional medical device, with a high conformance with the healthcare indexes. And the respiration rate and heartbeat rate can be simply calculated after tracking peaks in the frequency domain or zero-crossing detector in time domain with low relative error since it has big amplitude and long duration.

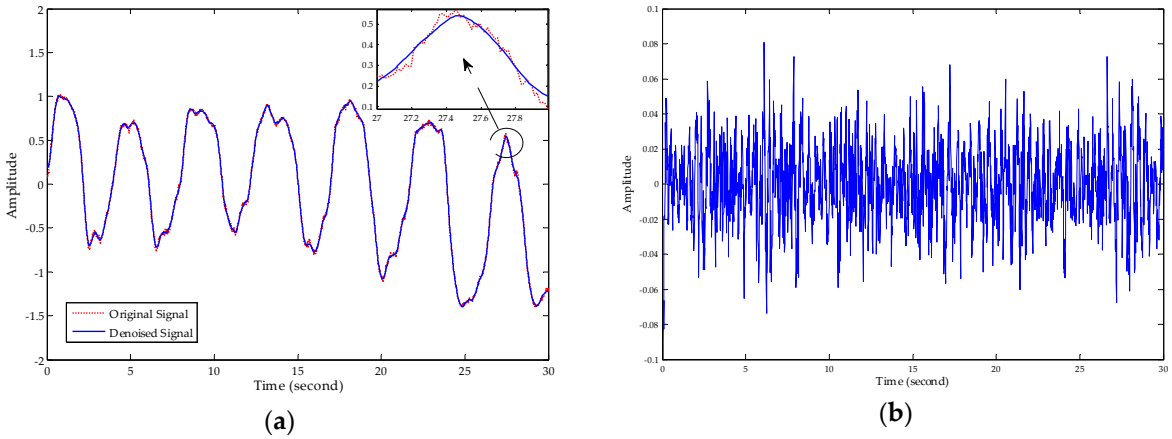

(**a**) (**b**)

Figure 11. Performance of denosing using proposed method. (**a**) Comparison of original vital sign signal with the denoised signal. (**b**) The noise IMFs removed after denoising processing.

Preprints (www.preprints.org) | NOT PEER-REVIEWED | Posted: 25 August 2016 doi:10.20944/preprints201608.0206.v1

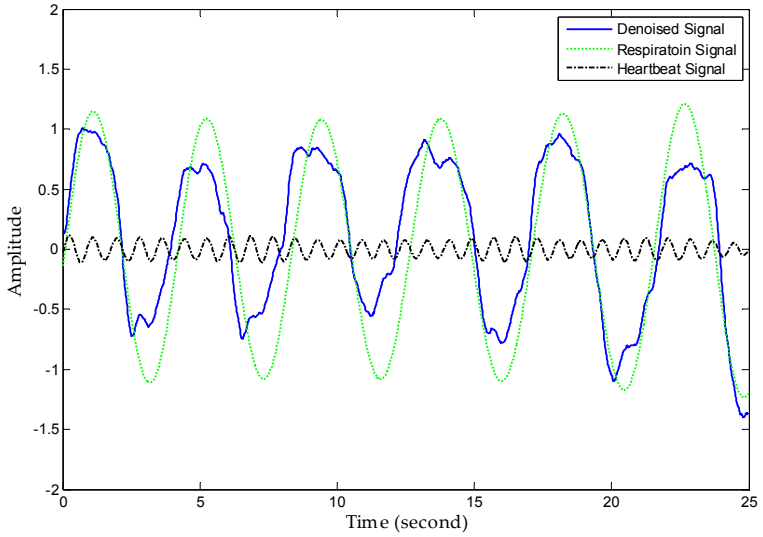

Figure 12. Performance of separating the signal using proposed method.

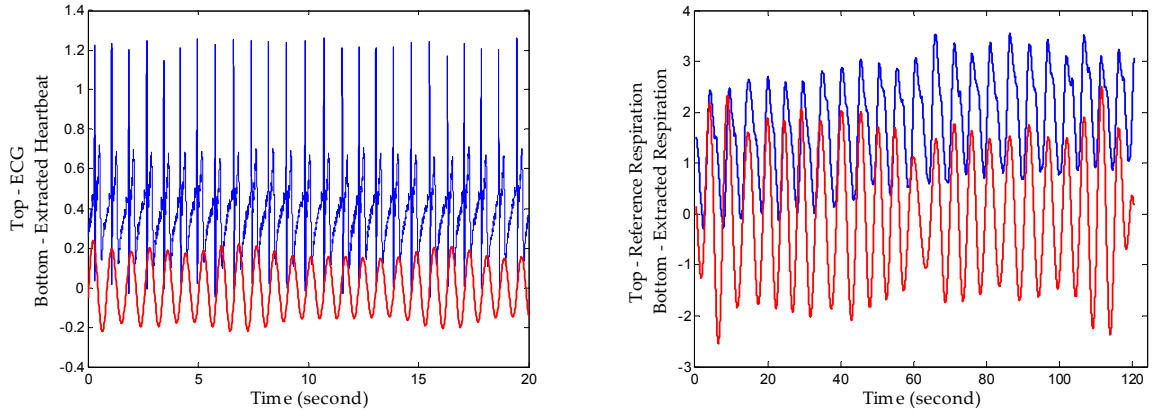

(**a**) (**b**)

Figure 13. Extracted signal compared with reference signal. (**a**) Extracted heartbeat signal and ECG reference signal. (**b**) Extracted respiration signal and respiration reference signal.

6. Conclusions

This paper describes a new application of an IR-UWB radar sensor and methods for non-contact detection of the vital signs of human subjects. This compact IR-UWB radar system combined with proposed signal processing algorithms can detect subject respiration signals and heartbeat signals. In most of the previous studies, the CW Doppler radar was used for detecting vital signs of human subjects, which should be used within the range band, and had no signs for accurate range measurement. When we apply the IR-UWB technology into vital sign sensing application, it not only eliminates power consumption and system complexity at the cost of affordable price, but also captures the high range resolution with vital signs due to the benefit of UWB information.

When the radar works, the interferences caused by indoor targets and antennas crosstalk are very serious and common. In this case, the SNR of the radar echo signal was low, and it was difficult to extract respiration signals from the complicated background noise. In order to minimize the clutter caused by environmental objects, some methods were used for improving the SNR in this paper. Proposed signal processing methods involving clutter removal, denosing based EEMD and separating respiration signals with heartbeat signals, are used one after another, so that the SNR of respiration and heartbeat increase by 7.59 dB and 4.82 dB, respectively, compared with traditional FIR filter method. Our experimental results show that the respiration signals and heartbeat signals

can be extracted well. As future work, more biomedical parameters like HR and HRV will be tested together to check the feasibility of our proposed medical sensor system and the signal processing methods.

Acknowledgments: This work was supported by the National Natural Science Foundation of China under Grant 61271441. The authors would like to thank the Key Lab. of Medical Digital Imaging Technology, Harbin Institute of Technology Shenzhen Graduate School, for their permission to use their ECG device.

Author Contributions: Each author contributed extensively to the preparation of this manuscript. Xikun Hu developed the sensor hardware system and carried out the experiments. Tian Jin developed the algorithms. All authors participated in the discussion about the proposal and contributed to the analysis of the results.

Conflicts of Interest: The authors declare no conflict of interest. The founding sponsors had no role in the design of the study; in the collection, analyses, or interpretation of data; in the writing of the manuscript, and in the decision to publish the results.

References

1. Watson-Watt, *R. Radar in War and in Peace*. Nature 1945, 155, 319–324.
2. Lin, J.C. Non-invasive microwave measurement of respiration. IEEE Proc. 1975.
3. Skolnik, M.I. *Introduction to radar. In Radar Handbook 2*. McGraw-Hill Company: New York, NY, USA, 1962; pp. 1–18.
4. Li, C.; Lin, J.; Xiao, Y. Robust overnight monitoring of human vital signs by a non-contact respiration and heartbeat detector. In Proceedings of the 28th Annual International Conference of the IEEE, New York, NY, USA, 31 August–3 September 2006; pp. 2235–2238.
5. Yilmaz, T.; Foster, R.; Hao, Y. Detecting Vital Signs with Wearable Wireless Sensors. *Sensors* **2010**, 10, 10837–10862.
6. Cianca, E.; Gupta, B. FM-UWB for communications and radar in medical applications. *Wireless Personal Communications*. **2009**, 51, 793-809.
7. Yarovoy, A.G.; Matuzas, J.; Levitas, B.; Ligthart, P. UWB radar for human being detection. *IEEE Aero. El. Sys. Mag.* **2005**, 21, 22-26.
8. Hussain, M.G.M. Ultra-Wideband Impulse Radar: An overview of the Principles. *IEEE Aero. El. Sys. Mag.* **1998**, 13, 9-14.
9. Fontana, R.J. Recent system applications of short-pulse ultra-wideband (UWB) technology. *IEEE Trans. Microw. Theory Tech*. **2004,** 52**,** 2087-2104.
10. Zhang, C.; Kuhn, M.-J.; Merkl, B.-C.; Fathy, A.-E.; Mahfouz, M.-R. Real-time noncoherent UWB positioning radar with millimeter range accuracy: Theory and experiment. I*EEE Trans. Microw. Theory Tech.* **2010**, 58, 9–20.
11. Taylor, J.D. *Ultra-Wideband Radar Technology*. CRC Press, 2001.
12. Wang, Y.; Yang, Y.; Fathy, A.E. Reconfigurable ultra-wide band see-through-wall imaging radar system. In Proceedings of the 2009 IEEE Antennas and Propagation Society International Symposium, North Charleston, SC, USA, 1–5 June 2009; pp. 1–4.
13. Yan, J.; Z., H.; Li, Y.; Sun, L.; Hong. H.; Zhu X. Through-the-Wall Human Respiration Detection Usi ng Impulse Ultra-wide-band Radar. In *Biomedical Wireless* Technologies, Networks, and Sensing Systems (BioWireleSS), Proceedings of the 2016 IEEE Topical Conference, Austin, TX, USA, 24-27 January 2016; pp. 94-96.
14. Anghel, A.; Vasile, G.; Cacoveanu, R.; Ioana, C.; Ciochina, S. Short-Range Wideband FMCW Radar for Millimetric Displacement Measurements. *IEEE Trans. Geosci. Remote Sens.* **2014**, 52, 5633–5642.
15. Taylor, J.D. Ultra-Wideband Radar Application and Design, CRC Press, 2012, 373-387.
16. McEwan, T.E. Body monitoring and imaging apparatus and method. US Patent 5.573.012. November 1996.
17. Staderini, E.M. Oral presentation: Medical applications of UWB radars. July 2008.
18. McEwan, T.E.; Azevedo, S. Micropower impulse radar. *Science and Technology: Review*. **1996**, 16–29.
19. Staderini, E.M. UWB radars in medicine. *IEEE Aero. El. Sys. Mag.* **2002**, 17, 13-18.
20. Ossberger, G.; Buchegger, T.; Schimback, E.; Stelzer, A.; Weigel, R.; Non-invasive respiratory movement detection and monitoring of hidden humans using ultra wideband pulse radar. In the Proceeding of the

2004 International Workshop on Ultra Wideband Systems Joint with Conference on Ultra Wideband Systems and Technologies, Kyoto, Japan, 18-21 May 2004; pp. 395–399.

21. Venkatesh, S.; Anderson, C.; Rivera, N.V.; Buehrer, R.M. Implementation and analysis of respiration-rate estimation using impulse-based UWB. In 2005 IEEE Military Communications Conference (MILCOM 2005), 17- 20 October 2005; pp. 3314–3320.
22. Bilich, C.G. Bio-medical Sensing using Ultra Wideband Communications and Radar Technology: A Feasibility Study. In *IEEE Pervasive Health Conference and Workshops*, 19, 29 November - 01 December 2006; pp. 1-9.
23. Lazaro, A.; Girbau, D.; Villarino, R. Analysis of Vital Signs Monitoring Using an IR-UWB Radar, Progress In Electromagnetics Research, *PIER* **2010**, 100, 265-284.
24. Khan, F.; Choi, J.W.; Cho, S.H. Vital Sign Monitoring of a Non-stationary Human Through IR-UWB Radar. In Proceeding of 2014 IEEE International Conference on Network Infrastructure and Digital Content (IC-NIDC 2014), Beijing, China, 19-21 September 2014; pp. 511-514.
25. Huang, X.; Sun, L.; Tian, T.; Huang Z.; Clancy, E. Real-time noncontact infant respiratory monitoring using UWB radar. In the 16th IEEE International Conference on Communication Technology (ICCT), Hangzhou, China, 18-21 October 2015; pp.493-496.
26. Singh, M.; Ramachandran, G. Reconstruction of sequential cardiac in-plane displacement patterns on the chest wall by laser speckle interferometry. *IEEE Trans. Biomed. Eng*. **1991**, 38, 483-489.
27. Xu, Y; Dai, S; Wu, S; Chen, J; Fang, G. Vital Sign Detection Method Based on Multiple Higher Order Cumulant for Ultrawideband Radar. *IEEE Trans. Geosci. Remote*. **2012,** 50, 1254-1265.
28. Huang, N.E. et al. The Empirical Mode Decomposition and the Hilbert Spectrum for Nonlinear and Non-Stationary Time Series Analysis. *Proceedings: Mathmatical, Physical and Engineering Sciences*. **1998,** 454, 903–995.
29. Wu, Z.; Huang, N. E. Ensemble empirical mode decomposition: A noise-assisted data analysis method. *Adv. Adapt. Data Anal*. **2009**, 01, 1–41.
30. Torres, M. E.; Colominas, M.A.; Schlotthauer, G.; Flandrin, P. A Complete Ensemble Empirical Mode Decomposition with Adaptive Noise. In 2011 IEEE International Conference on Accoustics, Speech and Signal Processing (ICASSP), 22-27 May 2011; pp. 4144-4147.
31. Li, C.; Chen, F; Jin, J.; Lv, H.; Li, S.; Lu, G.; Wang, J. A Method for Remotely Sensing Vital Signs of Human Subjects Outdoors. *Sensors* **2014,** 15, 14830-14844.
32. Baboli, M.; Ghorashi, S.A.; Saniei, N.; Ahmadian, A. A New Wavelet Based Algorithm for Estimating Respiratory Motion Rate Using UWB Radar. In Proceeding of the 2009 International Conference on Biomedical and Pharmaceutical Engineering (ICBPE), Singapore, 2-4 December 2009; pp. 1-3.
33. Hjortland, H.A.; Wisland, D.T.; Lande, T.S.; Limbodal, C.; Meisal, K. Thresholded Samples for UWB Impulse Radar. In *IEEE International Symposium on Circuits and Systems (ISCAS)*, 27-30 May 2007; pp. 1210-1213.
34. Novelda. NV A620x Preliminary Datasheet. Novelda, October 2013.
35. Available online: https://en.m.wikipedia.org/wiki/Morlet_wavelet (accessed on 7 August 2016).
36. Lazaro, A.; Girbau, D.; Villarino, R. Techniques for Clutter Suppression in the Presence of Body Movements during the Detection of Respiratory Activity through UWB Radars. *Sensors* **2014**, 14, 2595–2618.